Journal of Solid State Chemistry 185 (2012) 10–17

Contents lists available at SciVerse ScienceDirect

Journal of Solid State Chemistry

journal homepage: www.elsevier.com/locate/jssc

Quadruple-layered perovskite $(CuCl)Ca_2NaNb_4O_{13}$

A. Kitada [a,b], Y. Tsujimoto [a,b], T. Yamamoto [a,b], Y. Kobayashi [a], Y. Narumi [c,d], K. Kindo [c], A.A. Aczel [e], G.M. Luke [e], Y.J. Uemura [f], Y. Kiuchi [c], Y. Ueda [c], K. Yoshimura [b], Y. Ajiro [a], H. Kageyama [a,b,g,h,*]

[a] Department of Energy and Hydrocarbon Chemistry, Faculty of Engineering, Kyoto University, Nishikyo, Kyoto 615-8510, Japan
[b] Department of Chemistry, Graduate School of Science, Kyoto University, Kyoto 606-8502, Japan
[c] Institute for Solid State Physics, University of Tokyo, Kashiwa, Chiba 277-8581, Japan
[d] Institute for Materials Research, Tohoku University, Katahira 2-1-1, Sendai 980-8577, Japan
[e] Department of Physics and Astronomy, McMaster University, Hamilton, Ontario, Canada L8S 4M1
[f] Department of Physics, Columbia University, New York, NY 10027, USA
[g] Institute for Integrated Cell-Material Sciences, Kyoto University, Sakyo, Kyoto 606-8501, Japan
[h] CREST, Japan Science and Technology Agency, Kawaguchi 332-0012, Japan

ARTICLE INFO

Article history:
Received 3 January 2011
Received in revised form
20 October 2011
Accepted 24 October 2011
Available online 29 October 2011

Keywords:
Crystal structure
Magnetism
Ion-exchange reaction
Quadruple-layered perovskite
Two-dimensional magnet
$(CuCl)Ca_2NaNb_4O_{13}$

ABSTRACT

We will present the synthesis, structure and magnetic properties of a new quadruple-layered perovskite $(CuCl)Ca_2NaNb_4O_{13}$. Through a topotactic ion-exchange reaction with $CuCl_2$, the precursor $RbCa_2NaNb_4O_{13}$ presumably having an incoherent octahederal tliting changes into $(CuCl)Ca_2NaNb_4O_{13}$ with a $2a_p \times 2a_p \times 2c_p$ superstructure (tetragonal; $a=7.73232(5)$ Å, $c=39.2156(4)$ Å). The well-defined superstructure for the ion-exchanged product should be stabilized by the inserted $CuCl_4O_2$ octahedral layers that firmly connect with neighboring perovskite layers. Magnetic studies show the absence of long-range magnetic ordering down to 2 K despite strong in-plane interactions. Aleksandrov's group theory and Rietveld refinement of synchrotron X-ray diffraction data suggest the structure to be of $I4/mmm$ space group with in-phase tilting along the a and b axes, a two-tilt system ($++0$).

© 2011 Elsevier Inc. All rights reserved.

1. Introduction

The discovery of high-T_c superconducting layered cupric oxides has led to the search for phenomena driven by quantum fluctuations in two-dimensional (2D) $S=1/2$ antiferromagnets with square and analogous lattices. Examples include the J_1-J_2 lattice (where J_1 and J_2 denote the nearest and next-nearest exchange constants, respectively) $Li_2VO(Si, Ge)O_4$ [1], the 1/5-depleted lattice CaV_4O_9 [2], and the Shastry–Sutherland lattice $SrCu_2(BO_3)_2$ [3]. These quantum spin systems exhibit unconventional behaviors at low temperatures; e.g., spin-disordered ground state and quantized magnetization, but there still remain many open issues unsolved. For example, no material has been obtained to represent a theoretically predicted resonating-valence-bond (RVB) state in the J_1-J_2 model [4], in which spin-singlets are quantum mechanically resonating among themselves.

$(CuCl)LaNb_2O_7$ belongs to a family with the general formula $(CuX)A_{n-1}B_nO_{3n+1}$ (X: Cl^-, Br^-; A: La^{3+}, Ca^{2+}, Sr^{2+}, …; B: Nb^{5+}, Ta^{5+}, Ti^{4+}; $n=2$, 3), all prepared by topotactic ion-exchange reactions using Dion–Jacobson type layered perovskite oxides as a host. The magnetic CuX planes in $(CuX)A_{n-1}B_nO_{3n+1}$ carrying $S=1/2$ are well separated spatially by nonmagnetic $A_{n-1}B_nO_{3n+1}$ perovskite slabs (~11 Å for $n=2$ and ~15 Å for $n=3$) [5–7]. As a result, various exotic quantum phenomena emerge depending on constituent elements; $(CuCl)LaNb_2O_7$ has a product of spin-singlet dimers as the ground state [8–12], and $(CuBr)LaNb_2O_7$ and $(CuCl)LaTa_2O_7$ order magnetically in a stripe spin structure with significantly reduced magnetic moments [13,14]. The solid solution $(CuCl)La(Nb_{1-x}Ta_x)_2O_7$ shows a quantum phase separation at low temperatures between the spin-singlet and the antiferromagnetic states [14,15]. $(CuBr)A_2B_3O_{10}$ has a 1/3 quantized plateau in the magnetization curve, the width of which is varied by the in-plane lattice size [16].

In $(CuX)A_{n-1}B_nO_{3n+1}$, n is the parameter that controls the two-dimensionality of the magnetic characters. It is well known that increased two-dimensionality enhances quantum fluctuations in some cases, leading to a spin-disordered (paramagnetic) state stabilized even at low temperatures relative to the exchange constant. For example, the 2D kagomé compound $Ba_2Sn_2Ga_3ZnCr_7O_{22}$, which contains a magnetically inert spacer of $Ba_2Sn_2Ga_2O_{12}$ (9.4 Å thick), has an extraordinarily large frustration factor of 200 [17]. Unfortunately, the preparation of $(CuX)A_{n-1}B_nO_{3n+1}$ has been exclusively limited to $n=2$ and 3 cases. This paper will deal with the

* Corresponding author at: Kyoto University, Department of Energy and Hydrocarbon Chemistry, Nishikyo, Kyoto 615-8510, Japan. Fax: +81753832510.
E-mail address: kage@scl.kyoto-u.ac.jp (H. Kageyama).

0022-4596/$ - see front matter © 2011 Elsevier Inc. All rights reserved.
doi:10.1016/j.jssc.2011.10.038

synthesis, structure and magnetism of a new $n=4$ compound, $(CuCl)Ca_2NaNb_4O_{13}$, prepared by ion-exchange of $RbCa_2NaNb_4O_{13}$. Doubling along all the crystallographic axes has been observed, which could be attributed to an octahedral tilting of the type (++0) in Glazer notation. Moreover, magnetic experiments show that the system stays in a paramagnetic state down to 2 K despite strong in-plane exchange couplings.

2. Experimental

2.1. Synthesis

The preparation of the precursor $RbCa_2NaNb_4O_{13}$, a quadruple-layered Dion–Jacobson phase as illustrated in Fig. 1, follows that of an earlier work [18]. First, a triple-layered phase $RbCa_2Nb_3O_{10}$ was prepared from appropriate mixture of Rb_2CO_3 (rare metallic, 99.9%), $CaCO_3$ (rare metallic, 99.99%) and Nb_2O_5 (rare metallic, 99.99%) [19], where 50% molar excess of Rb_2CO_3 was used to compensate for loss due to its vaporization. $RbCa_2Nb_3O_{10}$ was washed with distilled water after the calcinations, and dried at 120 °C overnight. $NaNbO_3$ was prepared from appropriate mixtures of Na_2CO_3 (rare metallic, 99.9%) and Nb_2O_5 (rare metallic, 99.99%) with 5% molar excess of Na_2CO_3. Then, equimolar $RbCa_2Nb_3O_{10}$ and $NaNbO_3$ were mixed and heated at 1150 °C for 24 h in air to yield $RbCa_2NaNb_4O_{13}$. Finally, a low-temperature ion-exchange reaction expressed as

$$RbCa_2NaNb_4O_{13} + CuCl_2 \rightarrow (CuCl)Ca_2NaNb_4O_{13} + RbCl \quad (1)$$

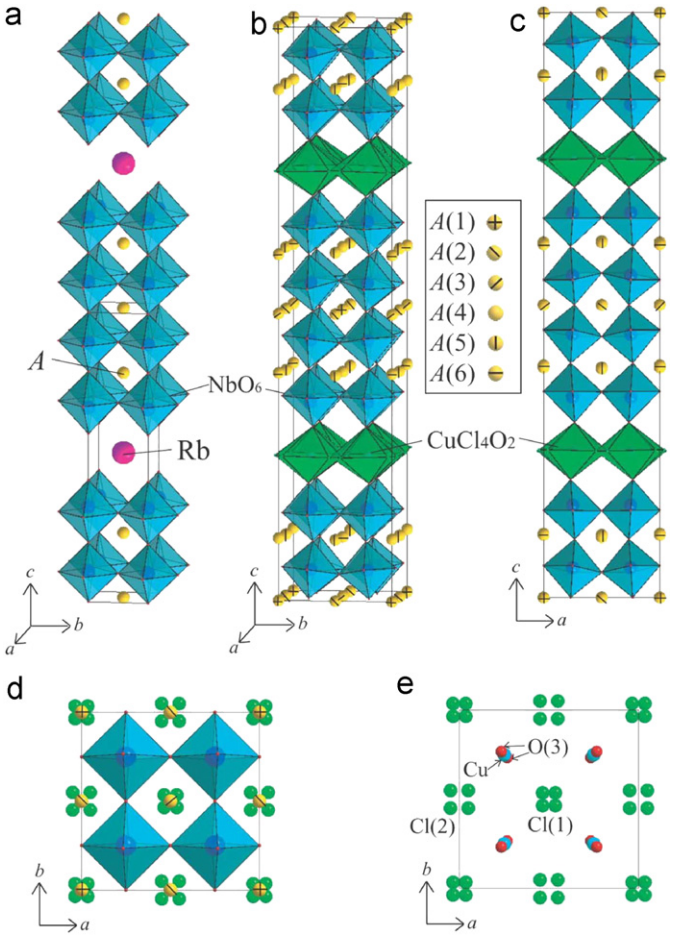

Fig. 1. (a) Clinographic presentation of the structure of $RbCa_2NaNb_4O_{13}$ reported by Sugimoto et al. [18] and (b) the room-temperature structure of $(CuCl)Ca_2NaNb_4O_{13}$ obtained in this study. (c) [010] projection, (d) [001] projection and (e) the edge-shared $CuCl_4O_2$ layer viewed along [001].

was performed. Here, $RbCa_2NaNb_4O_{13}$ was mixed with a 2-fold molar excess of ultra dry $CuCl_2$ (Sigma-Aldrich, 99.999%), pressed into a pellet with a hand press inside an argon-filled glovebox, and heated at 320 °C for 7 day in a sealed, evacuated ($<10^{-3}$ Torr) Pyrex tube. The final product was washed with distilled water to eliminate the excess copper chloride and the rubidium chloride by-product, and dried at 120 °C overnight.

2.2. Chemical characterization

Chemical analysis was based on energy dispersive X-ray spectroscopy (EDS) measurements of sets of individual grains. These were carried out on a JEOL (JSM-5600) scanning electron microscope equipped with an EDS system installed at the Institute for Solid State Physics (ISSP), the University of Tokyo. Transmission electron microscopy (TEM) experiments were carried out at room temperature with an operating voltage of 200 kV using a JEM2010F system at ISSP. Specimens of the host and the ion-exchanged compound were finely ground in methanol and then placed on a Cu microgrid mesh for TEM observation. Synchrotron powder X-ray diffraction (XRD) experiments were carried out at ambient temperature on a large Debye–Scherrer camera installed at BL02B2 at the Japan Synchrotron Radiation Research Institute SPring-8 using an imaging plate as a detector. Incident beams from a bending magnet were monochromatized to 0.77747 Å. The final product was contained in a glass capillary tube with an inner diameter of 0.2 mm and was rotated during measurements to eliminate the effect of preferential orientation. The diffraction data were collected in a 2θ range from 1° to 75° with a step interval of 0.01°. Rietveld refinement was performed using the RIETAN-2000 program [20]. The agreement indices used were the weighted profile $R_{wp}=[\Sigma w_i(y_{io}-y_{ic})^2/\Sigma w_i(y_{io})^2]^{1/2}$ and the goodness of fit (GOF), $\chi^2=(R_{wp}/R_{Bragg})^2$, where $R_{Bragg}=[(N-P)/\Sigma w_i y_{io}^2]^{1/2}$, y_{io} and y_{ic} are the observed and calculated intensities, respectively, w_i is the weighting factor, N the total number of y_{io} data when the background is refined, and P the number of adjusted parameters.

2.3. Magnetism

Magnetic susceptibility measurements of $(CuCl)Ca_2NaNb_4O_{13}$ were performed on a powder sample with a Quantum Design MPMS (Magnetic Property Measurement System) over a temperature range $T=2$–350 K in a magnetic field H of 1 T. High-field magnetization measurements up to 57 T were conducted using an induction method with a multilayer pulse magnet installed at ISSP. Specific heat measurements were performed by the heat relaxation method down to 2 K in a zero magnetic field using a Quantum Design PPSM (Physical Property Measurement System) at ISSP. Zero-filed and longitudinal-field muon spin relaxation (muSR) measurements were performed at the M20 channel at TRIUMF, the Canadian National Accelerator Laboratory in Vancouver. Polarized positive muons were implanted one-by-one into the specimen mounted in a gas-flow He cryostat down to $T=2.0$ K. Details of the muSR methods can be found elsewhere [21].

3. Results and discussion

3.1. Structure

Laboratory XRD patterns of both $RbCa_2NaNb_4O_{13}$ and $(CuCl)Ca_2NaNb_4O_{13}$ at room temperature could be readily indexed into tetragonal systems with cell parameters $a=3.869$ Å and $c=18.859$ Å for the former and $a=3.866$ Å and $c=19.608$ Å for the latter compound. No impurity phase could be detected within the experimental resolution limits. The obtained lattice parameters

for the precursor are in a good accordance with the reported values (a=3.8727 Å, c=18.9116 Å) [18]. The elongation along the c axis, ca. 0.7 Å relative to the precursor, is consistent with the results on the n=2 and 3 compounds [5–7] and thus is evidence for the insertion of a CuCl layer. The EDS experiment reveals the composition of the final product to be approximately Cu:Cl:Ca:Na:Nb=1:1:2:1:4. The absence of Rb also supports the occurrence of desired ion-exchange reaction (1).

The use of electron diffraction is crucial for identifying possible superstructures. The room-temperature electron diffraction (ED) patterns for $(CuCl)Ca_2NaNb_4O_{13}$ along the [001]* and [010]* zone axes are shown in Fig. 2a and b, which reveal weak commensurate reflections such as (1/2 1/2 0) and (1/2 0 1/2), together with strong fundamental ones. The extinct reflections are described as {hkl; $h+k+l$=odd}, {hk0; $h+k$=odd}, {h00; h=odd}, {h0l; $h+l$=odd} and {00l; l=odd} in the $2a_p \times 2a_p \times 2c_p$ cell indexation, where a_p and c_p denote the original primitive unit cell parameters of $RbCa_2NaNb_4O_{13}$. Furthermore, the room-temperature synchrotron XRD profile (see the inset of Fig. 3) not only confirmed the tetragonal symmetry, but also detected superlattice reflections being consistent with the extinction conditions obtained from the TEM study. Therefore, possible space groups are $I4$ (No. 79), $I-4$ (No. 82), $I4/m$ (No. 87), $I422$ (No. 97), $I4mm$ (No. 107), $I-4m2$ (No. 119), $I-42m$ (No. 121) and $I4/mmm$ (No. 139).

A large number of perovskite-based compounds have structural deviations from their ideal structure, which is governed by the tolerance factor t. When t is smaller than unity, coherent octahedral tilting takes place, resulting in reduction of symmetry accompanied by the emergence of a superstructure [22]. Assuming a random distribution of Ca^{2+} and Na^+ for $(CuCl)Ca_2NaNb_4O_{13}$, one can use, in a first approximation, the average value t=0.955 ($r(Ca^{2+})$=1.34 Å, $r(Na^+)$=1.39 Å [23]). It is therefore natural to consider that octahedral tilting is present in this material and causes the doubling of all the crystallographic axes.

It is then presumed that $RbCa_2NaNb_4O_{13}$ with the identical t value exhibits the same type of octahedral tilting, which, however, was not reported. We conducted synchrotron XRD and TEM measurements of this compound. While the XRD experiments did not detect any superreflection peaks (not shown), the ED displayed very weak and diffuse superlattice reflections (Fig. 4a). These reflections were observed only in a small region of the particle, and in other regions no obvious superlattice

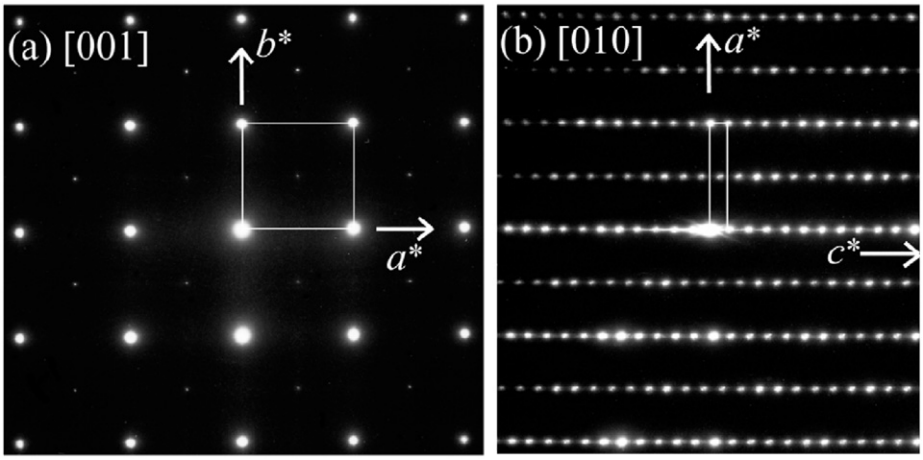

Fig. 2. Electron diffraction patterns of $(CuCl)Ca_2NaNb_4O_{13}$ at room temperature obtained along (a) the [001]- and (b) the [010]-zone axes.

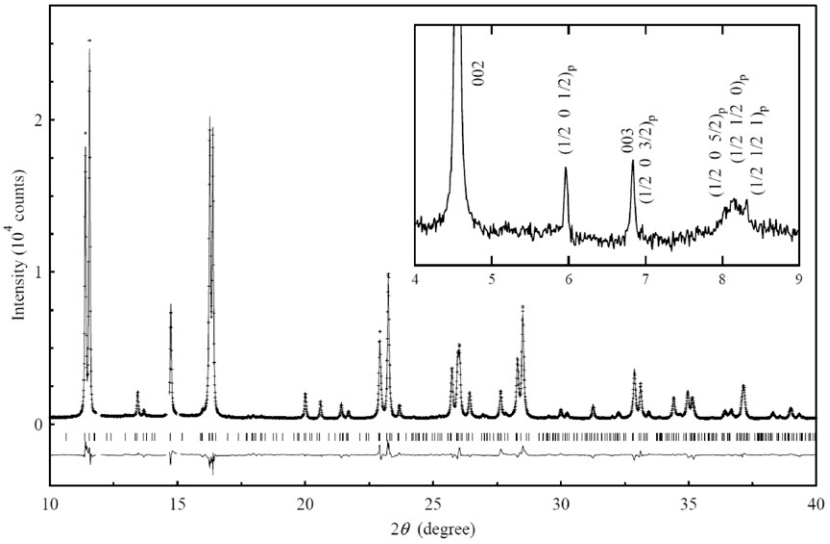

Fig. 3. Powder synchrotron X-ray diffraction profile of $(CuCl)Ca_2NaNb_4O_{13}$ obtained at room temperature. The wavelength was λ=0.77747 Å. Observed and calculated diffraction patterns are represented by crosses and solid curve, respectively. Vertical bars are related to the calculated Bragg reflection positions and solid lines below are the difference between observed and calculated data. The inset shows several superreflections to evidence the $2a_p \times 2a_p \times 2c_p$ supercell.

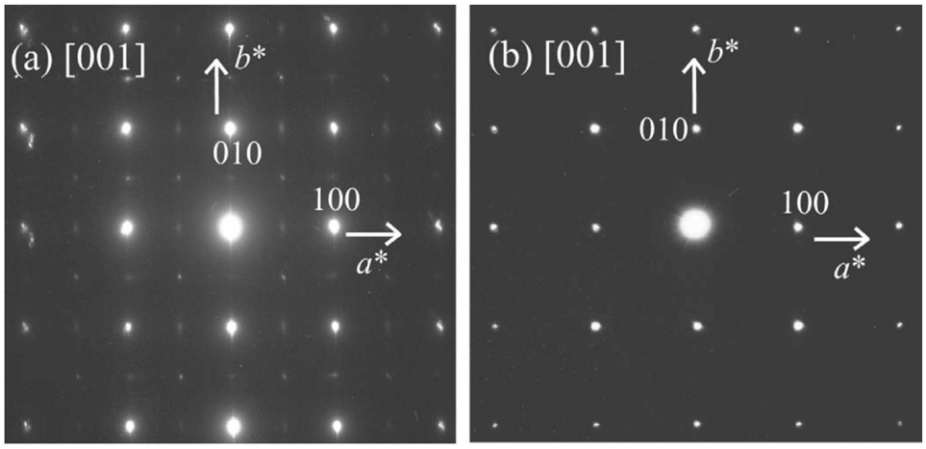

Fig. 4. (a) and (b) Room-temperature electron diffraction patterns along the [0 0 1]-zone axis of $RbCa_2NaNb_4O_{13}$ obtained from different areas.

reflections were observed (Fig. 4b). This observation is in contrast to $(CuCl)Ca_2NaNb_4O_{13}$, the ED of which has well-defined super-reflections (without any streaks) observed uniformly across the specimen (Fig. 2a and b). This means that the inserted copper-halide arrays in between the perovskite layers play a crucial role in stabilizing the superstructure associated with the octahedral tilting.

The difference in structure between $RbCa_2NaNb_4O_{13}$ and $(CuCl)Ca_2NaNb_4O_{13}$ would be related to the difference in the bonding nature connecting adjacent perovskite blocks. In $RbCa_2NaNb_4O_{13}$, the adjacent $Ca_2NaNb_4O_{13}$ blocks are weakly bound via the Rb cations. The weak bonding nature of this and related Dion–Jacobson layered perovskites is indeed what provides the abilities of ion-exchange and makes them amenable to exofoliation into nanosheets [24]. However, this feature in turn results in the octahedral tilting being extended to only a short distance. In $(CuCl)Ca_2NaNb_4O_{13}$, the adjacent perovskite slabs are connected covalently via the edge-shared $CuCl_4O_2$ octahedra, which results in a long ranged coherent octahedral tilting. The details of the possible octahedral tilting arrangements will be discussed later.

3.2. Magnetic properties

Fig. 5a shows the temperature dependence of magnetic susceptibility χ for $(CuCl)Ca_2NaNb_4O_{13}$. At the first sight, it does not show any spectacular behavior. With decreasing temperature down to 2 K, the susceptibility gradually increases. The Curie–Weiss fit, $\chi = C/(T-\theta)$, above 150 K gives a Curie constant $C=0.386$ emu K/mol Cu, which agrees well with that expected for 1 mol of Cu^{2+} ions (0.375 emu K/mol when assuming the isotropic g-factor of 2.0). It also confirms a successful ion-exchange reaction. Below 150 K, the experimental susceptibility deviates from the Curie–Weiss behavior. The Weiss temperature is $\theta=22.4$ K (Fig. 5b). The positive Weiss temperature is suggestive of ferromagnetic intra-layer interactions. The out-of-plane interaction is expected to be negligibly small because the magnetic layer is widely separated by the nonmagnetic layer ($\sim$20 Å). This implies that the magnetization would saturate easily by applying a weak magnetic field. Contradictory to this prediction, however, the magnetization curves of $(CuCl)Ca_2NaNb_4O_{13}$ at 1.3 K and 4.2 K evolve rather slowly and do not saturate even at 57 T (Fig. 6). This indicates the presence of a strong antiferromagnetic exchange coupling at low temperatures, and the apparent small (and ferromagnetic) Weiss temperature is as a consequence of close competition between ferromagnetic and antiferromagnetic interactions within the CuCl layer. The coexistence of such competing interactions in the CuBr and CuCl layers have been discussed in the

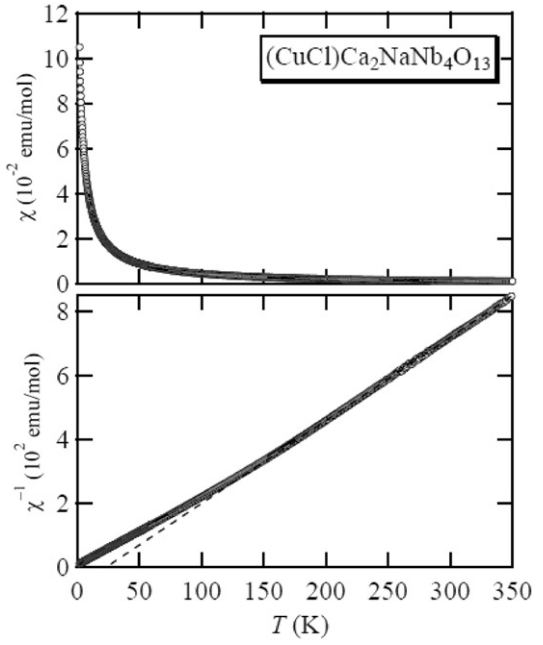

Fig. 5. (a) Susceptibility and (b) inverse susceptibility for $(CuCl)Ca_2NaNb_4O_{13}$ measured at 1 T. The dotted line represents the Curie–Weiss fit.

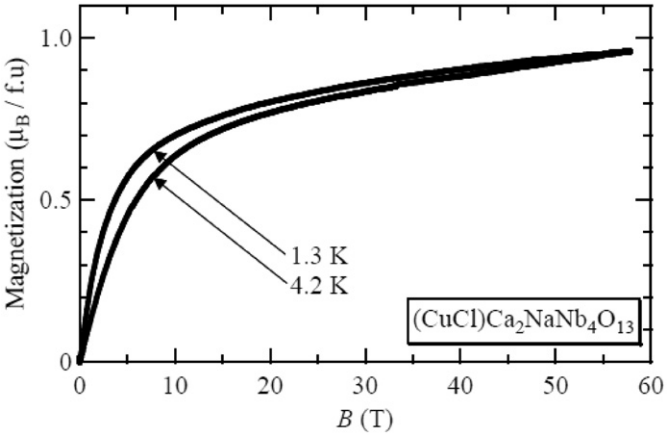

Fig. 6. High field magnetizations for $(CuCl)Ca_2NaNb_4O_{13}$ at 1.3 K and 4.2 K measured in pulsed fields. Within the experimental certainty, no hysteresis was observed between runs where the field was increased/decreased.

$n=2$ and $n=3$ systems [8,12–16], so it is not surprising that this situation is present in the present $n=4$ case.

The presence of competing interactions in the CuCl layer is inferred also from the temperature dependence of total specific heat. As shown in Fig. 7, C_p/T exhibits a Schottky-like round maximum at around 3 K. This anomaly might be due to an energy gap of some type, although $(CuCl)Ca_2NaNb_4O_{13}$ does not have any spin-singlet ground state with a finite gap (see Figs. 5a and 6). Interestingly, similar behavior is reported for a 2D kagomé compound $[Cu_3(titmb)_2(OCOCH_3)_6]\cdot H_2O$ (titmb=1,3,5-tris(imidazol-1-ylmethyl)-2,4,6 trimethylbenzene) with competing interactions also within the layer [25]. Competing interactions create a very large density of low-lying excited states, where even a small perturbation may change its ground state, giving non-spin-gapped aspects in susceptibility and/or magnetization data.

MuSR measurements offer a unique opportunity in detecting static magnetic order with high sensitivity. Fig. 8 shows the zero-field spectra for $(CuCl)Ca_2NaNb_4O_{13}$ measured at 5 K and 2 K. The time evolution $A(t)$ of the muon spin polarization was obtained from the time histograms $F(t)$ and $B(t)$ of the forward and backward counters as

$$A(t)=A_0G(t)=[F(t)-B(t)]/[F(t)+B(t)] \quad (2)$$

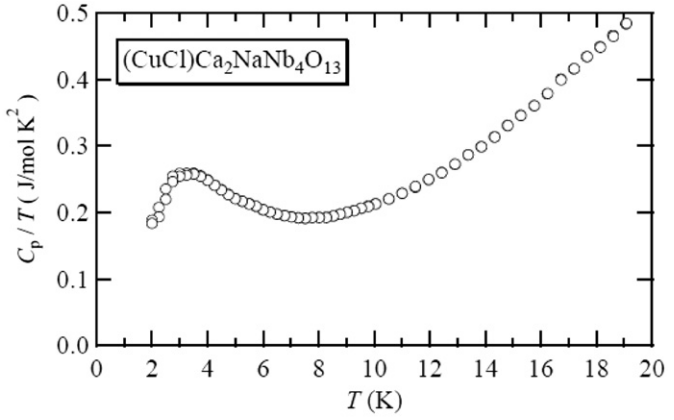

Fig. 7. Temperature dependence of C_p/T for $(CuCl)Ca_2NaNb_4O_{13}$, showing a Schottky anomaly at around 3 K.

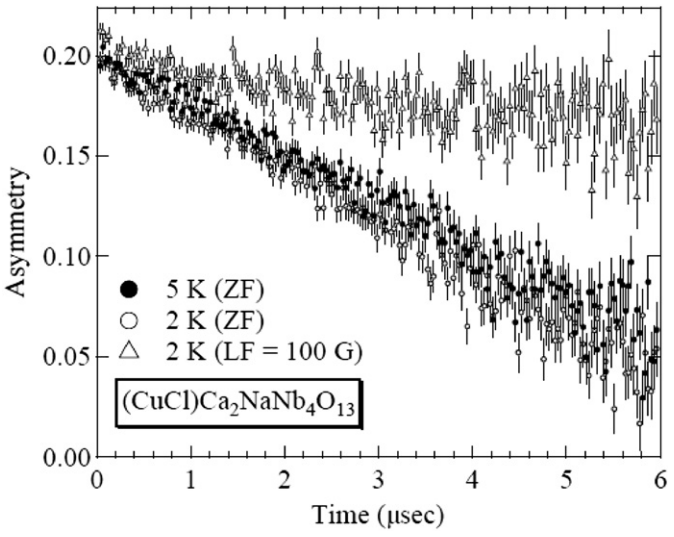

Fig. 8. Time evolution of muSR asymmetry in zero field (ZF) for $(CuCl)Ca_2NaNb_4O_{13}$ measured at 2 K and 5 K. The decoupled spectrum in a longitudinal field (LF) of 100 G at 2 K is also shown.

where A_0 is a constant and $G(t)$ represents the relaxation function defined with $G(0)=1$ [21]. The relaxation spectra at 5 K and 2 K are almost identical and can be decoupled by the longitudinal magnetic field of 100 G. These results unambiguously demonstrate that long-range magnetic order is absent down to 2 K, despite strong in-plane interactions. The absence of magnetic order down to 2 K is attributed to the competing interactions within the layer as well as the enhanced two-dimensionality. Further study is required to understand the nature of the ground state in $(CuCl)Ca_2NaNb_4O_{13}$.

3.3. Structural refinement

As we mentioned above, eight possible tetragonal space groups for $(CuCl)Ca_2NaNb_4O_{13}$ are derived from the XRD and ED patterns. However, solving the structure solely by Rietveld analysis without any further constraints would be very difficult, given that the $2a_p\times 2a_p\times 2c_p$ unit cell contains as 176 atoms ($Z=8$). For this reason, we utilize Aleksandrov's analysis of symmetry reduction in response to octahedral tilting in layered perovskites [26]. Our material finds the following characteristics: an even number of perovskite layers (i.e., $n=4$), $P4/mmm$ in the absence of octahedral tilting, and a $2a_p\times 2a_p\times 2c_p$ cell. These conditions reduce the possible space groups to $P4_2/mmc$ (No. 131) with a $(+++)$ tilt, $P4_2/nmc$ (No. 137) with a $(++-)$ tilt and $I4/mmm$ (No. 139) with a $(++0)$ tilt, where $+$, $-$ and 0 denote, respectively, in-phase tilt, out-of-phase tilt and no tilt in Glazer's notation [27]. Among them, only $I4/mmm$ meets the extinction conditions derived from the TEM and XRD results.

Therefore, Rietveld refinement of the synchrotron XRD data for $(CuCl)Ca_2NaNb_4O_{13}$ was performed using $I4/mmm$ as the space group. Initial atomic coordinates of calcium, sodium, niobium and oxygen were set based on crystallographic data of $RbCa_2NaNb_4O_{13}$ ($P4/mmm$, $a_p\times a_p\times c_p$) reported by Sugimoto et al. [18]. Calcium and sodium ions were assumed to be randomly distributed at the A-sites. The thermal parameters of Cl, A(Ca, Na), Nb and O atoms were set to be equal, a constraint being sometimes applied when complex structures are refined, as in $RbCa_2NaNb_4O_{13}$ [18]. Linear constraints were logically set up so as to maintain the $(++0)$ tilt system: $x(O(i))=x(O(j))$ for i, $j=1$–3 and $y=0.25$ for O(4)∼O(7). The initial positions of copper atom and chlorine atoms were set at the ideal (most symmetric) positions: 8f (1/4, 1/4, 1/4) for Cu, and 4e (0, 0, z) and 4d (0, 1/2, 1/4) for Cl(1) and Cl(2), respectively. The refinement converged quickly to acceptable agreement factors ($R_{wp}=5.90\%$, $R_{Bragg}=3.25\%$ and $\chi^2=3.31$). However, obtained thermal parameters for chlorine atoms were too large, $B_{iso}(Cl)=8.2(3)$ Å^2, a result similar to previous structural studies on the homologous $(CuCl)A_{n-1}B_nO_{3n+1}$ [5,6].

We subsequently modified the model by introducing disorder of chlorine atoms. Several models involving disorder of the chlorine sites were examined and the model in which Cl(1) and Cl(2) atoms moved to, respectively, 16m (x, x, z) and 16k (x, $x+1/2$, 1/4), with 25% site occupancy, resulted in the best fit: $x=0.035(9)$ for Cl(1) and 0.049(9) for Cl(2), $B_{iso}(Cl)=2.8(5)$ Å^2, $R_{wp}=5.72\%$, $R_{Bragg}=3.25\%$ and $\chi^2=3.10$. We would like to note that the z-coordinate of the Cl(1) atom was very close to 0.25 ($z=0.252(1)$), indicating that the Cl(1) atom hardly moved off the Cu-plane. The obtained thermal parameters for each site were acceptable considering previous data on perovskite niobates [18,28,29]. The observed, calculated, and difference plots for the final refinement are shown in Fig. 3, and the crystallographic data are presented in Table 1. The structure is illustrated in Fig. 1b–e. Note that, when the thermal parameters of Cl, A(Ca, Na), Nb and O atoms were individually refined, the variable atomic coordinates became less stable. Given many adjustable parameters, it is hard, with the current synchrotron data alone, to perform a refinement

Table 1
Crystallographic data for $(CuCl)Ca_2NaNb_4O_{13}$.

	Atom	Site	x	y	z	g	B_{iso} (Å^2)
$(CuCl)Ca_2NaNb_4O_{13}$	Cu	8*f*	0.25	0.25	0.25	1	1.26(9)
*I*4/*mmm*	Cl(1)	16*m*	0.535(9)	0.535(9)	0.252(1)	0.25	2.8(5)
$a=7.73232(5)$ Å	Cl(2)	16*k*	0.049(9)	0.549(9)	0.25	0.25	2.8(5)
$c=39.2156(4)$ Å	*A*(1)	2*a*	0	0	0	1	1.71(7)
$R_{wp}=5.72\%$	*A*(2)	4*c*	0	0.5	0	1	1.71(7)
$R_{Bragg}=3.25\%$	*A*(3)	2*b*	0.5	0.5	0	1	1.71(7)
$\chi^2=3.10$	*A*(4)	4*e*	0	0	0.108(2)	1	1.71(7)
	A(5)	8*g*	0	0.5	0.107(2)	1	1.71(7)
	A(6)	4*e*	0.5	0.5	0.103(1)	1	1.71(7)
	Nb(1)	16*m*	0.249(1)	0.249(1)	0.0545(1)	1	0.02(1)
	Nb(2)	16*m*	0.251(1)	0.251(1)	0.15774(4)	1	0.02(1)
	O(1)	8*h*	0.233(2)	0.233(2)	0	1	2.29(9)
	O(2)	16*m*	0.233(2)	0.233(2)	0.0997(3)	1	2.29(9)
	O(3)	16*m*	0.233(2)	0.233(2)	0.2011(3)	1	2.29(9)
	O(4)	16*n*	0	0.25	0.0543(4)	1	2.29(9)
	O(5)	16*n*	0	0.25	0.1487(8)	1	2.29(9)
	O(6)	16*n*	0	0.25	0.0428(4)	1	2.29(9)
	O(7)	16*n*	0	0.25	0.1478(8)	1	2.29(9)

without the constraints on the thermal parameters. In order to validate the structure proposed in this study, high-resolution neutron diffraction study, which can determine oxygen positions with higher accuracy, along the combined X-ray/neutron refinement would be necessary.

The bond distances are listed in Table 2. It is seen that the Nb(2)–O(3) distance of 1.712(13) Å (O(3) is the outer oxygen site) is relatively short. However, we would like to note that in layered perovskite niobates, the Nb–O bond extending to the interlayer has a tendency to form a shorter bond. For example, similar values of 1.77(6) Å and 1.748(6) Å were reported, respectively, for $RbCa_2NaNb_4O_{13}$ [18] and $KCa_2Nb_3O_{10}$ [30]. The bond valence sum (BVS) method was applied to estimate the valences of cations using tabulated parameters [31], and we obtained +1.7, +5.5 and +1.4 for Cu, Nb and *A* ($=Ca_{2/3}Na_{1/3}$), respectively, in reasonable agreement with the formal values.

The Cl(1) atom, which the O(3) atom moves toward from the ideal site, has a smaller degree of displacement from its ideal position than the Cl(2) atom (see Fig. 1e), probably to reduce Coulomb's repulsion from the apical oxygen. By contrast, the Cu atom, which has its neighboring two apical oxygen atoms O(3) moving away along ⟨110⟩, remains at the midpoint of these two oxygen atoms i.e. the ideal site. It should be noted that at low temperatures, ordering of the chlorine atoms might occur. Such structural relationships between $CuCl_4O_2$ and NbO_6 octahedra are also reported in the $n=2$ analog $(CuCl)LaNb_2O_7$ [12]. In $(CuCl)LaNb_2O_7$, the Cl ions as well as their nearest oxygen atoms shift mostly along the b_p axis, probably due to their electrostatic repulsion. Moreover, in marked contrast to the $n=4$ case, the Cu atoms are displaced from their ideal positions, while the apical oxygen atoms still move toward the same direction.

It is now interesting to compare the present compound with the *A*-site deficient perovskite $Na_{0.74}WO_3$, which is the only reported compound with the same (++0) tilt [32]. We found that the tilt angle φ along the *a*-axis (estimated from $\tan\varphi=\{a\cdot(x(O(i))-x(O(j)))\}/\{c\cdot(z(O(i))-z(O(j)))\}$ where $(i,j)=(1,2)$ and $(2,3)$) was 4.0°, which is close to 3.40° in $Na_{0.74}WO_3$ [32]. Note that this value is much smaller than that in $RbAgF_3$ with a (− − +) tilt (8.0°) [33] and $SrZrO_3$ with a (00−) tilt (8.95°) [34], despite having similar *t* values. As pointed out in Ref. [22], the *A*-site (Na) in $Na_{0.74}WO_3$ has three kinds of coordination geometry; i.e. square-planar, rectangular-planar and square-prismatic coordination. Likewise, for $(CuCl)Ca_2NaNb_4O_{13}$ the *A*(1)-, *A*(2)- and *A*(3)-sites comprising the inner perovskite slabs being surrounded only by $Nb(1)O_6$ octahedra, have, respectively, square-planar, rectangular-planar and square-prismatic coordinations (Fig. 9a–c). Note, however, that the *A*(4)–*A*(6)-sites comprising the outer perovskite slabs being surrounded both by $Nb(1)O_6$ and $Nb(2)O_6$ octahedra have a more distorted coordination geometry as shown in Fig. 9d–f.

Table 2
Bond distances for $(CuCl)Ca_2NaNb_4O_{13}$.

Bond	Bond distances (Å)
Cu–Cl(1)	2 × 2.34(11)
	4 × 2.76(1)
Cu–Cl(2)	2 × 2.19(10)
	4 × 2.78(2)
Cu–O(3)	2 × 2.1925(13)
Nb(1)–O(4)	2 × 1.937(11)
Nb(1)–O(2)	1 × 1.939(11)
Nb(1)–O(6)	2 × 1.957(11)
Nb(1)–O(1)	1 × 1.986(2)
Nb(2)–O(3)	1 × 1.712(13)
Nb(2)–O(7)	2 × 1.963(9)
Nb(2)–O(5)	2 × 1.973(9)
Nb(2)–O(2)	1 × 2.283(10)
A(1)–O(1)	4 × 2.554(18)
A(1)–O(4)	8 × 2.876(13)
A(2)–O(6)	4 × 2.560(10)
A(2)–O(1)	4 × 2.739(1)
A(2)–O(4)	4 × 2.876(13)
A(3)–O(6)	8 × 2.560(10)
A(3)–O(1)	4 × 2.913(18)
A(4)–O(5)	4 × 2.483(46)
A(4)–O(4)	4 × 2.886(59)
A(4)–O(2)	4 × 2.936(9)
A(5)–O(7)	2 × 2.508(39)
A(5)–O(5)	2 × 2.532(49)
A(5)–O(2)	4 × 2.754(6)
A(5)–O(4)	2 × 2.829(45)
A(6)–O(2)	4 × 2.558(3)
A(6)–O(7)	4 × 2.600(49)

4. Conclusion

We synthesized the quadruple-layered copper oxyhalide $(CuCl)Ca_2NaNb_4O_{13}$. Through topotactic ion-exchange with $CuCl_2$, the precursor $RbCa_2NaNb_4O_{13}$ with diffuse superreflections changes into $(CuCl)Ca_2NaNb_4O_{13}$ with a well-defined, tetragonal

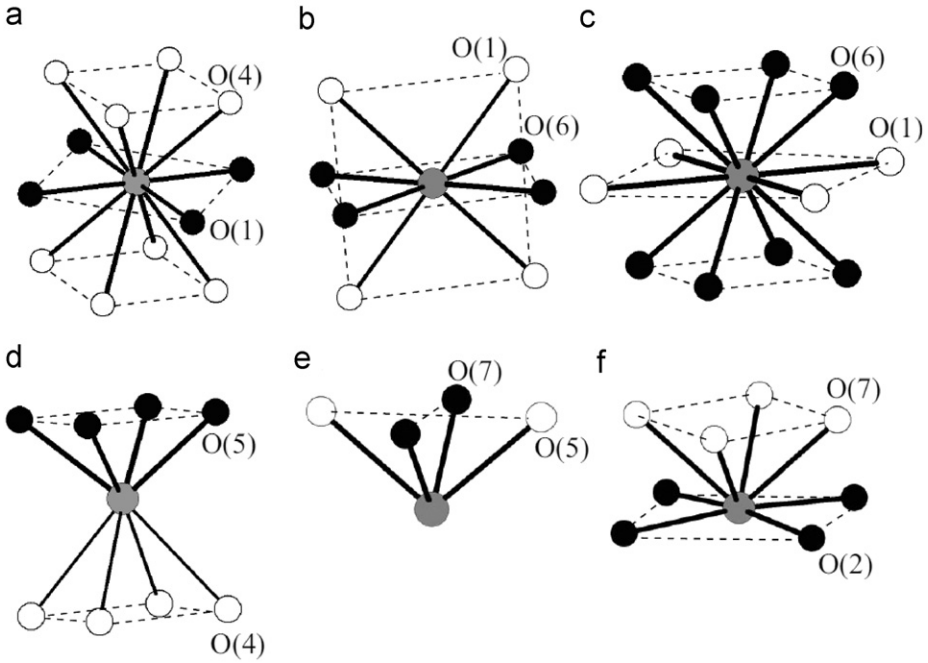

Fig. 9. Coordination environment of the *A*-site cation in $(CuCl)Ca_2NaNb_4O_{13}$. The lightly shaded circles represent the *A*-site cations. The filled circles with the thicker solid lines represent the nearest oxygen atoms and the open circles with the thinner solid lines the second coordination sphere. The dotted lines are guides for the eye. (a) *A*(1); (b) *A*(2); (c) *A*(3); (d) *A*(4); (e) *A*(5); and (f) *A*(6).

$2a_p \times 2a_p \times 2c_p$ superstructure. The insertion of the edge-shared $CuCl_4O_2$ layer induces strong bonding between the neighboring perovskite slabs, likely stabilizing the superstructure. Magnetic studies reveal that $(CuCl)Ca_2NaNb_4O_{13}$ does not undergo magnetic long-range ordering down to 2 K despite strong magnetic interaction in the CuCl plane, due to the enhanced quantum fluctuations in two dimensions. Group theory analysis together with the synchrotron XRD and TEM measurements suggests the *I*4/*mmm* space group with an unusual in-phase two-tilt system (++0) in $(CuCl)Ca_2NaNb_4O_{13}$. Applying the ion-exchange reaction to other layered perovskites $A'A_{n-1}B_nO_{3n+1}$ with $n > 4$ may allow us to obtain more two-dimensional materials with further enhanced quantum fluctuations.

Acknowledgments

The synchrotron radiation experiments were performed at SPring-8 with the approval of the Japan Synchrotron Radiation Research Institute. This work was supported by Grants-in-Aid for Science Research (Nos. 19052004 and 22245009) from the Ministry of Education, Culture, Sports, Science and Technology (MEXT) of Japan, by CREST. This work was also supported by the Global COE Program "Integrated Material Science" (No. B-024) from MEXT of Japan, by Murata Science Foundation, and by the Japan-U.S. Cooperative Science Program (No. 14508500001) from JSPS and NSF. The work at Columbia was supported by US National Science Foundation grant for Materials World Network, DMR-05–02706 and DMR-08–06846. One of the authors (A.K.) was supported by JSPS for Young Scientists.

References

[1] R. Melzi, P. Carretta, A. Lascialfari, M. Mambrini, M. Troyer, P. Mittlet, F. Mila, Phys. Rev. Lett. 85 (2000) 1318.
[2] K. Kodama, H. Harashina, H. Sasaki, Y. Kobayashi, M. Kasai, S. Taniguchi, Y. Yasui, M. Sato, K. Kakurai, T. Mori, M. Nishi, J. Phys. Soc. Jpn. 66 (1997) 793.
[3] H. Kageyama, M. Nishi, N. Aso, K. Onizuka, T. Yoshihama, K. Nukui, K. Kodama, K. Kakurai, Y. Ueda, Phys. Rev. Lett. 84 (2000) 5876.
[4] P.W. Anderson, Mater. Res. Bull. 8 (1973) 153.
[5] T.A. Kodenkandath, J. Lalena, W.L. Zhou, E.E. Carpenter, C. Sangregorio, A.U. Falster, W.B. Simmons Jr., C.J. O'Connor, J.B. Wiley, J. Am. Chem. Soc. 121 (1999) 10743.
[6] T.A. Kodenkandath, A.S. Kumbhar, W.L. Zhou, J.B. Wiley, Inorg. Chem. 40 (2001) 710.
[7] H. Kageyama, L. Viciu, G. Caruntsu, Y. Ueda, J.B. Wiley, J. Phys. Condens. Matter 16 (2004) S585.
[8] H. Kageyama, T. Kitano, N. Oba, M. Nishi, S. Nagai, K. Hirota, L. Viciu, J.B. Wiley, J. Yasuda, Y. Baba, Y. Ajiro, K. Yoshimura, J. Phys. Soc. Jpn. 74 (2005) 1702.
[9] H. Kageyama, J. Yasuda, T. Kitano, K. Totsuka, Y. Narumi, M. Hagiwara, K. Kindo, Y. Baba, N. Oba, Y. Ajiro, K. Yoshimura, J. Phys. Soc. Jpn. 74 (2005) 3155.
[10] A. Kitada, Z. Hiroi, Y. Tsujimoto, T. Kitano, H. Kageyama, Y. Ajiro, K. Yoshimura, J. Phys. Soc. Jpn. 76 (2007) 093706.
[11] M. Yoshida, N. Ogata, M. Takigawa, J. Yamaura, M. Ichihara, T. Kitano, H. Kageyama, Y. Ajiro, K. Yoshimura, J. Phys. Soc. Jpn. 76 (2007) 104703.
[12] C. Tassel, J. Kang, C. Lee, O. Hernandez, Y. Qiu, W. Paulus, E. Collet, B. Lake, T. Guidi, M.-H. Whangbo, C. Ritter, H. Kageyama, S.-H. Lee, Phys. Rev. Lett. 105 (2010) 167205.
[13] N. Oba, H. Kageyama, T. Kitano, J. Yasuda, Y. Baba, M. Nishi, K. Hirota, Y. Narumi, M. Hagiwara, K. Kindo, T. Saito, Y. Ajiro, K. Yoshimura, J. Phys. Soc. Jpn. 75 (2006) 113601.
[14] A. Kitada, Y. Tsujimoto, H. Kageyama, Y. Ajiro, M. Nishi, Y. Narumi, K. Kindo, M. Ichihara, Y. Ueda, Y.J. Uemura, K. Yoshimura, Phys. Rev. B 80 (2009) 174409.
[15] Y.J. Uemura, A.A. Aczel, Y. Ajiro, J.P. Carlo, T. Goko, D.A. Goldfeld, A. Kitada, G.M. Luke, G.J. MacDougall, I.G. Mihailescu, J.A. Rodriguez, P.L. Russo, Y. Tsujimoto, C.R. Wiebe, T.J. Williams, T. Yamamoto, K. Yoshimura, H. Kageyama, Phys. Rev. B 80 (2009) 174408.
[16] Y. Tsujimoto, H. Kageyama, Y. Baba, A. Kitada, T. Yamamoto, Y. Narumi, K. Kindo, M. Nishi, J.P. Carlo, A.A. Aczel, T.J. Williams, T. Goko, G.M. Luke, Y.J. Uemura, Y. Ueda, Y. Ajiro, K. Yoshimura, Phys. Rev. B 78 (2008) 214410.
[17] I.S. Hagemann, Q. Huang, X.P.A.. Gao, A.P. Ramirez, R.J. Cava, Phys. Rev. Lett. 86 (2001) 894.
[18] W. Sugimoto, H. Ohkawa, M. Naito, Y. Sugahara, K. Kuroda, J. Solid State Chem. 148 (1999) 508.
[19] M. Dion, M. Ganne, M. Tournoux, Mater. Res. Bull. 16 (1981) 1429.
[20] F. Izumi, T. Ikeda, Mater. Sci. Forum. 321–324 (2000) 198.
[21] R.S. Hayano, Y.J. Uemura, J. Imazato, N. Nishida, T. Yamazaki, R. Kubo, Phys. Rev. B 20 (1979) 850.
[22] P.M. Woodward, Acta Crystallogr. B 53 (1997) 44.
[23] R.D. Shannon, Acta Crystallogr. A 32 (1976) 751.
[24] R.E. Shaak, T.E. Mallouk, Chem. Mater. 14 (2002) 1455.
[25] Y. Narumi, K. Katsumata, Z. Honda, J.-C. Domenge, P. Sindzingre, C. Lhuillier, Y. Shimaoka, T.C. Kobayashi, K. Kindo, Europhys. Lett. 65 (2004) 705.

[26] K.S. Aleksandrov, Crystallogr. Rep. 40 (1995) 251.
[27] A.M. Glazer, Acta Crystallogr. B 28 (1972) 3384.
[28] M. Yashima, S. Matsuyama, R. Sano, M. Itoh, K. Tsuda, D. Fu, Chem. Mater. 23 (2011) 1643.
[29] J.A. Schottenfeld, A.J. Benesi, P.W. Stephens, G. Chen, P.C. Eklund, T.E. Mallouk, J. Solid State Chem. 178 (2005) 2313.
[30] H. Fukuoka, T. Isami, S. Yamanaka, J. Solid State Chem. 151 (2000) 40.
[31] I.D. Brown, D. Altermatt, Acta Crystallogr. B 41 (1985) 244.
[32] C.N.W. Darlington, J.A. Hriljac, K.S. Knight, Acta Crystallogr. B 59 (2003) 584.
[33] R.H. Odenthal, R. Hoppe, Monatsh. Chem. 102 (1971) 1340.
[34] A. Ahtee, M. Ahtee, A.M. Glazer, A.W. Hewat, Acta Crystallogr. B 32 (1976) 3243.